THE JOURNAL OF PHYSICAL CHEMISTRY Letters

Letter

Cite This: J. Phys. Chem. Lett. 2018, 9, 2791−2796

pubs.acs.org/JPCL

Origin of Vibrational Instabilities in Molecular Wires with Separated Electronic States

Giuseppe Foti* and Héctor Vázquez*

Institute of Physics, Academy of Sciences of the Czech Republic, Cukrovarnicka 10, Prague, Czech Republic

Supporting Information

ABSTRACT: Current-induced heating in molecular junctions stems from the interaction between tunneling electrons and localized molecular vibrations. If the electronic excitation of a given vibrational mode exceeds heat dissipation, a situation known as vibrational instability is established, which can seriously compromise the integrity of the junction. Using out of equilibrium first-principles calculations, we demonstrate that vibrational instabilities can take place in the general case of molecular wires with separated unoccupied electronic states. From the *ab initio* results, we derive a model to characterize unstable vibrational modes and construct a diagram that maps mode stability. These results generalize previous theoretical work and predict vibrational instabilities in a new regime.

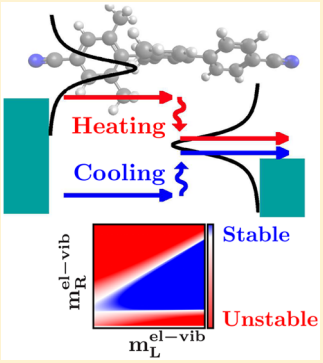

The theoretical understanding of electron transport in nanoscale systems has experienced significant advances in recent years.[1,2] In the field of molecular electronics, in particular, the balance between the energy released and absorbed by electrical current flowing through molecular junctions out of equilibrium represents an active topic of research since this energy transfer affects the stability of the system. Electrons can exchange energy with localized molecular vibrations[3−10] thus increasing or decreasing the junction effective temperature. The system is stable under an applied bias if a steady-state solution for the vibronic population can be found. However, due to the high current densities, the amount of energy transferred between the electronic system and vibrations of the molecule can lead to conformational changes[11−15] or molecular dissociation and breakdown of the junction.[16−18] Understanding heat generation and dissipation at the atomistic level is therefore not only of fundamental interest but also a prerequisite for the realization of nanoelectronic devices.

From a theoretical perspective, current-induced heating and cooling in molecular junctions has been extensively studied using different approaches. In model systems, inelastic excitation of molecular vibrations has been explored with both master equations[19−22] as well as Green's function techniques[23−26] while, for *ab initio* calculations, the latter method has been preferentially used.[27−31] The energy transferred from the electrical current to molecular vibrations can be dissipated through different channels such as anharmonic coupling between the modes of the molecule, the coupling to bulk phonons, or the electronic bath itself. When the current-induced heat generation overcomes cooling processes, the population of vibrational modes increases with time, a situation known as vibrational instability. Different mechanisms have been identified as possible origins of vibrational instabilities such as a high external bias or the suppression of electron−hole damping of molecular vibrational energy.[32] In a nonequilibrium situation, it has been demonstrated that the presence of nonconservative wind and Berry phase forces can also lead to an uncontrolled increase of vibron population and mode energy.[29,33,34] Theoretical works based on Green's functions techniques[7] and master equation approach[35] showed how a bias-driven population inversion of filled and empty states in molecular junctions with donor−acceptor structure, where the applied voltage lifts the occupied donor resonance above the empty acceptor state, could generate the conditions for negative vibrational damping and vibrational instability.

Here we perform a detailed analysis based on density functional theory (DFT) and nonequilibrium Green's function technique (NEGF) of the current-induced heating dynamics of a representative terphenyl molecular wire with separated empty electronic states. Despite the absence of a donor−acceptor structure or population inversion, DFT-NEGF reveals the presence of several unstable vibrational modes. Based on these results, we build a two-level model system that generalizes these findings. We find that vibrational instabilities are a more general phenomenon that does not require a donor−acceptor structure and should be applicable to molecular junctions that have LUMO-dominated transport and empty molecular orbitals separated on each side of the junction. This electronic separation can be achieved by chemical means (e.g., with donor−acceptor groups[7,36−38]) or, as exemplified here, from structural factors such as bulky steric groups, which give rise to

Received: March 28, 2018
Accepted: May 9, 2018
Published: May 9, 2018

DOI: 10.1021/acs.jpclett.8b00940
J. Phys. Chem. Lett. 2018, 9, 2791−2796

decreased π conjugation.[39,40] We show how, as the applied voltage modulates the offsets between left and right molecular states, emission processes can be enhanced, and vibrational instabilities can occur. From *ab initio* and model calculations, we analyze the electronic and vibrational properties that make vibrational modes unstable under bias, and derive a stability diagram for archetypal molecular junctions that generalizes the previous findings. Our calculations thus reveal, for the first time, the important role of the electron-vibration coupling matrix internal structure in the generation of instabilities.

Figure 1a shows the geometry studied in the present work. The molecule consists of a terphenyl wire with cyano groups at both ends. It is adsorbed on Au(111) electrodes with tetrameric tips. Two phenyl rings have CH_3 groups, whose steric repulsion increases the twist angle between these two rings to about 82°, decreasing the conjugation of the conducting π system[39,40] and electronically separating both sides of the junction. We introduce a third phenyl ring to generate a small splitting between the left and right states. The right-localized state is at a slightly lower energy since it is delocalized over two rings. Figure 1b illustrates the energy exchange processes between tunneling electrons and localized molecular vibrations. Electrons releasing energy as molecular vibrations (red arrow) heat the junction, while absorption of vibrations (blue arrows) increases the energy of the tunneling electrons, effectively cooling the junction. A two-level system can be constructed to model the molecular junction. Empty molecular states localized on either end of the molecule are represented by ϵ_L and ϵ_R and coupled to the respective electrode via a parameter τ. Both states interact weakly with each other through a hopping term t.

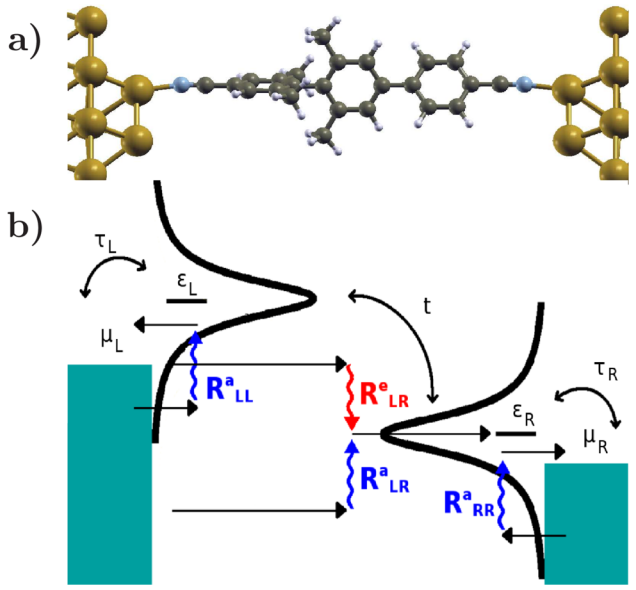

Figure 1. (a) Side view of a terphenyl molecule anchored to Au(111) electrodes with tetrameric terminations. The large twist angle between benzene rings induced by the steric repulsion of CH_3 groups results in separated π electronic states. (b) Schematic of a two-level system of the current-induced heating and cooling processes taking place in the junction.

These energy exchange mechanisms can be described by the following expression:[7,28,41,42]

$$R^{a,e,\lambda}_{\alpha,\beta} = \int_{\epsilon_i}^{\epsilon_f} \Lambda^{a,e,\lambda}_{\alpha,\beta}(\epsilon)d\epsilon \quad (1)$$

where the absorption and emission functions $\Lambda^{a,e,\lambda}_{\alpha,\beta}$ are

$$\Lambda^{a,e,\lambda}_{\alpha,\beta}(\epsilon) = \frac{1}{2\pi\hbar}\mathrm{Tr}[M^{\lambda}A_{\alpha}(\epsilon)M^{\lambda}A_{\beta}(\epsilon')] \quad (2)$$

Here, $\epsilon' = \epsilon \pm \hbar\omega_\lambda$. Superscripts "a,e" refer to absorption and emission, respectively, while indices α and β label the left and right electrodes. Notice the integration limits ϵ_i and ϵ_f in eq 1 are different for absorption and emission processes.[7,42] The rates for each mode λ also depend on energy ϵ and involve averaging the spectral functions $A_{\alpha,\beta}(\epsilon)$ over parallel electron momentum k.[42] In the undamped limit, the population of junction vibrations is given by[7]

$$N^{\lambda}(V_b) = \frac{R^{e,\lambda}(V_b)}{R^{a,\lambda}(V_b) - R^{e,\lambda}(V_b)} \quad (3)$$

where V_b is the applied bias voltage and $R^{a,\lambda}(V_b)$ is the sum of all absorption processes. As long as $R^{a,\lambda}(V_b) > R^{e,\lambda}(V_b)$, the population $N^{\lambda}(V_b)$ is positive, and, if the energy stored in the vibrational modes does not induce any change in the junction, the system is stable under an applied bias. However, if $R^{a,\lambda}(V_b) < R^{e,\lambda}(V_b)$, then $N^{\lambda}(V_b) < 0$, which means that a steady state solution for vibron populations cannot be found, and the system is unstable.[7,32,35]

Figure 2 shows the left- and right-projected spectral functions at 0 V (top panels) and 1.4 V (bottom panels) from the *ab initio* calculations. At equilibrium, the peaks of the left and right spectral functions are 0.25 eV apart, a splitting arising from being confined to one or two benzene rings, respectively. This separation of left and right states is also reflected in the different bias dependence of their spectral functions. A_L shifts with the left chemical potential μ_L, while A_R shifts with μ_R (the applied bias is split between both electrodes).

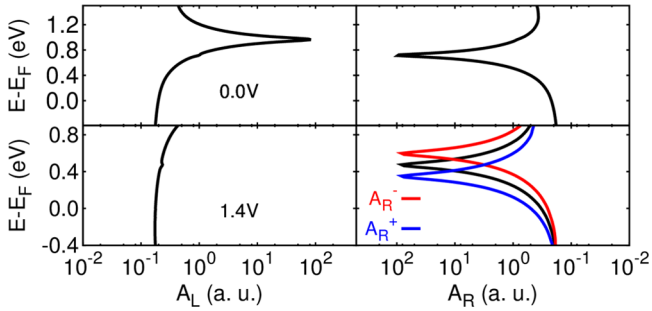

Figure 2. DFT-NEGF left- and right-projected spectral functions A_L and A_R calculated at 0.0 V (top panels) and at 1.4 V (bottom panels). Blue and red curves correspond to the right spectral functions shifted by the mode energy $A^{\pm}_R = A_R(\epsilon \pm \hbar\omega_\lambda)$, relevant for vibration absorption and emission processes.

The heating and stability of vibrational modes clearly depend on the external bias through the out-of-equilibrium self-consistent electronic structure and integration window [eq 1]. In the following, we consider V_b = 1.4 V, a voltage at which ϵ_R is inside the Fermi window, and we find several unstable modes. At 1.4 V, A_L has been shifted up in energy by almost 0.3 eV (its peak is at ~1.3 eV), while on the right side the peak of A_R moves down by a similar amount to approximately 0.5 eV. The red and blue curves in Figure 2 are the right spectral functions $A_R(\epsilon)$ shifted by the mode energy $\hbar\omega_\lambda$. Emission and

DOI: 10.1021/acs.jpclett.8b00940
J. Phys. Chem. Lett. 2018, 9, 2791−2796

absorption rates of molecular vibrations are proportional to $A_R(\epsilon - \hbar\omega_\lambda)$ and $A_R(\epsilon + \hbar\omega_\lambda)$, respectively [eq 2], affecting the energies at which emission and absorption reach their maxima. *Ab initio* calculations yield nine unstable vibrational modes at V_b = 1.4 V. Figure 3 shows the interelectrode emission and

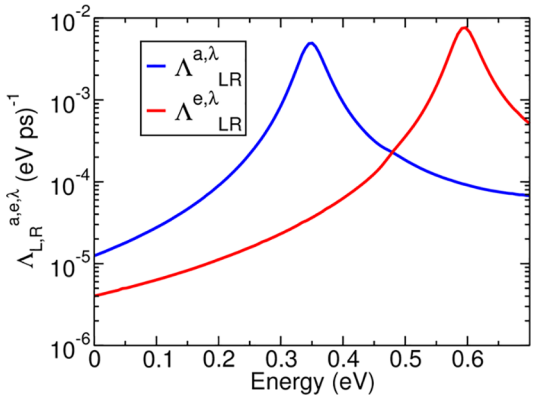

Figure 3. DFT-NEGF emission and absorption functions [eq 2] for unstable mode 2 at 1.4 V. Emission and absorption functions peak at $\epsilon_R + \hbar\omega_\lambda$ and $\epsilon_R - \hbar\omega_\lambda$, respectively. The higher peak value for emission indicates that the mode is potentially unstable under the applied bias.

absorption functions [eq 2] for one of these modes, which, as we discuss below, is a representative example of instability. The peak value of emission $\Lambda^{e,\lambda}_{L,R}$ is much greater than for absorption $\Lambda^{a,\lambda}_{L,R}$. Therefore, integration of these functions to calculate the rates [eq 1] yields a higher emission than absorption, and this mode is unstable. Intraelectrode absorption processes $\Lambda^{a,\lambda}_{L,L}$ and $\Lambda^{a,\lambda}_{R,R}$ are much smaller than interelectrode terms and do not reverse the mode instability. First-principles calculations confirmed that all unstable modes verify these two characteristics: (i) higher peak values of emission than interelectrode absorption functions ($\Lambda^{max,e,\lambda}_{L,R} > \Lambda^{max,a,\lambda}_{L,R}$), and (ii) mode (in)stability is not affected by intraelectrode terms.

To understand these findings and to distill the main physical mechanisms behind vibrational instabilities, we turn to the two-level model introduced in Figure 1b, which represents empty molecular states separated on either side of the junction. Details of the model are discussed in the Supporting Information. At a given bias voltage, only some vibrational modes are unstable. Therefore, we first discuss the characteristics of these unstable modes. In this two-level model, the expression for the emission and absorption functions [eq 2] is evaluated at two energies (A_L at ϵ, while A_R at $\epsilon \pm \hbar\omega_\lambda$). The expressions for A^L and A^R depend on the on-site energies (ϵ_L,ϵ_R), coupling to the electrodes (τ_L,τ_R) and the left−right coupling (t). We first fit the ab initio transmission spectrum at 1.4 eV to obtain these parameters, which allows us to compute A_L and A_R for the two-level model. Then, the elements of the model electron-vibration matrix $M^\lambda = (m^\lambda_{ij})$ are obtained for each unstable mode by fitting the ab initio emission and absorption rates $\Lambda^{a,\lambda}$ and $\Lambda^{e,\lambda}$. This two-step process accurately maps the first-principles elastic and the inelastic transport properties onto the two-level model.

The elements m^λ_{ij} (where, in this two-level system, the subscript labels the L and R sites) show how the different parameters of the model electronic structure are modulated by the movement of the different atoms induced by the mode: m^λ_{LL} represents the change in the on-site energy ϵ_L, while m^λ_{RR} refers to ϵ_R. The off-diagonal term $m^\lambda_{LR} = m^\lambda_{RL}$ is the change of the left−right coupling term t due to the movement of the dynamical atoms.

We find that for many unstable modes (including, e.g., for the mode in Figure 3), the expression of emission and absorption rates in eq 2 can be well approximated by just contributions of the form:

$$\Lambda^{a,e,\lambda}_{L,R}(\epsilon) \simeq \frac{1}{2\pi\hbar} \sum_{m,n,p,q,i,j=L,R} m^\lambda_{mn} m^\lambda_{pq} a^L_{LL}(\epsilon) a^R_{ij}(\epsilon') \quad (4)$$

where $\epsilon' = \epsilon + \hbar\omega_\lambda$ ($\epsilon' = \epsilon - \hbar\omega_\lambda$) for absorption (emission), and $a^{L,R}_{ij}(\epsilon)$ are the elements of the spectral matrices. For systems having separated electronic states with $\epsilon_L > \epsilon_R$, the emission function will have larger $a^L_{LL}(\epsilon)a^R_{ij}(\epsilon')$ products compared to the absorption function: $a^L_{LL}(\epsilon)$ increases with ϵ, and thus $a^L_{LL}(\epsilon)a^R_{ij}(\epsilon')$ products will be higher for emission processes (since $a^R_{ij}(\epsilon')$ peaks at higher energies $\epsilon' = \epsilon + \hbar\omega_\lambda$) than for absorption (where $a^R_{ij}(\epsilon')$ reaches its maximum at lower energies $\epsilon' = \epsilon - \hbar\omega_\lambda$). This provides an intuitive argument for why vibrational instabilities can be expected in molecules with separated empty electronic states without the need for population inversion. In molecular junctions, the density of states is still sloped around E_F after the position of resonances has been shifted with respect to DFT as a consequence of a more sophisticated description of electron interaction.[43]

Next, we generalize this analysis of vibrational instabilities. Figure 4 shows a stability diagram for a generic vibrational

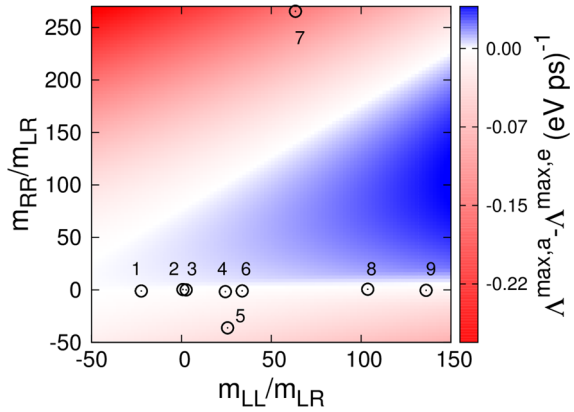

Figure 4. Stability diagram for a generic vibrational mode in a two-level system. Mode stability is given by the difference between absorption and emission maxima. Blue (red) regions represent stable (unstable) modes. The nine open symbols represent the unstable modes obtained from DFT-NEGF fitted to the two-level system.

mode with energy $\hbar\omega_\lambda$ equal to the average energy of all unstable modes in DFT-NEGF. The two-dimensional plot shows mode stability calculated using the two-level model for a wide range of values of diagonal elements m^λ_{ii} scaled to the average value of m^λ_{LR} across all nine unstable modes. The color represents the difference in peak heights $\Lambda^{max,a}_{L,R} - \Lambda^{max,e}_{L,R}$. Red regions correspond to the emission peak maximum being higher than that of absorption, and the mode (defined by the pair $\{m^\lambda_{LL}, m^\lambda_{RR}\}$) is unstable. Conversely, blue regions denote stable modes. The stability diagram constructed for the model system correctly describes the stability or instability of all modes computed from first-principles. Black circles represent the nine unstable modes found using DFT-NEGF. Many of these modes are distributed near the $m^\lambda_{RR}/m^\lambda_{LR} = 0$ axis,

DOI: 10.1021/acs.jpclett.8b00940
J. Phys. Chem. Lett. 2018, 9, 2791−2796

meaning that they induce only weak changes of the m^{λ}_{RR} parameter and instead modulate a wide range of values of the m^{λ}_{LL} term. These modes mostly comprise the leftmost and middle rings in Figure 1. Only in two cases does $m^{\lambda}_{RR}/m^{\lambda}_{LR}$ take large absolute values in modes that are more delocalized over the entire molecule or localized on the rightmost ring. Altogether, this analysis highlights that, for a given elastic transmission spectrum, the internal structure of the electron-vibration coupling matrix elements plays a fundamental role in the stability of the modes.

Having characterized unstable vibrational modes, we now discuss the role of electronic structure in mode stability using the model system constructed from DFT-NEGF. We use the energy and electron-vibration coupling matrix from one of the representative modes near the $m^{\lambda}_{RR}/m^{\lambda}_{LR} = 0$ region discussed above. The choice of this specific mode has little impact on our conclusions. We keep the electronic structure parameters $(\epsilon_R,\tau_L,\tau_R,t)$ fixed except ϵ_L, which we vary around ϵ_R. For each value, we calculate the difference in peak heights $\Lambda^{max,a}_{L,R} - \Lambda^{max,e}_{L,R}$. As before, we restrict the analysis to interelectrode terms, which we have seen to determine the (in)stability of the mode. Figure 5 shows the calculated mode stability as a function of $\epsilon_L - \epsilon_R$

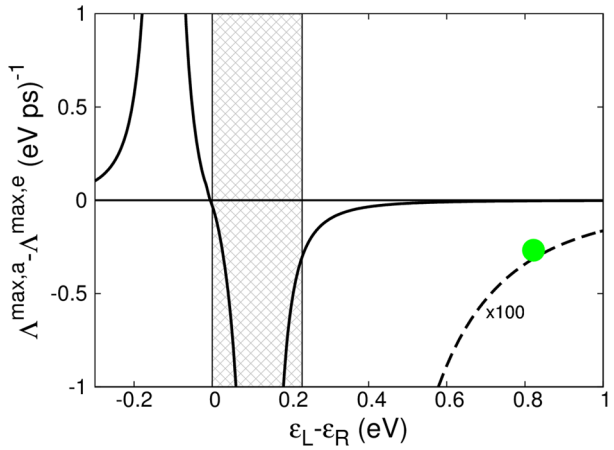

Figure 5. Difference between absorption and emission maxima $\Lambda^{max,a} - \Lambda^{max,e}$ as a function of the offset between left- and right-localized states for a representative vibrational mode. Positive (negative) values correspond to a stable (unstable) mode. The shaded area denotes the population inversion regime, with a strong instability at $\epsilon_L - \epsilon_R \simeq \hbar\omega_\lambda$. Negative values beyond $\epsilon_L - \epsilon_R = 0.23$ eV denote vibrational instabilities without the conditions of donor and acceptor states and population inversion. The filled symbol corresponds to DFT-NEGF.

for the mode labeled 2 in Figure 4, which was previously discussed. As ϵ_L is rigidly shifted, its occupation and offset with ϵ_R change. To the left of the vertical line at $\epsilon_L - \epsilon_R = 0.23$ eV, ϵ_L is below the left chemical potential, and the state is occupied. The region to the right of that line corresponds to an empty ϵ_L resonance. Since ϵ_R is kept at a fixed positive value, the shaded region between 0 and 0.23 eV defines the condition for population inversion. Positive values of $\Lambda^{max,a} - \Lambda^{max,e}$ correspond to a stable mode, while negative values indicate vibrational instabilities. The peak at $\epsilon_L - \epsilon_R = -0.12$ eV $\simeq -\hbar\omega_\lambda$ corresponds to efficient current-induced cooling arising from increased absorption: the energy of the vibration approximately matches the left−right level offset ($\epsilon_R \simeq \epsilon_L + \hbar\omega_\lambda$). This resonance condition greatly intensifies the absorption processes, which cool the junction, and thus $\Lambda^{max,a} - \Lambda^{max,e} \gg 0$.

For $\epsilon_L - \epsilon_R > 0$, $\Lambda^{max,a} - \Lambda^{max,e}$ is negative, indicative of an unstable junction. The dip at $\epsilon_L - \epsilon_R = +0.12$ eV $\simeq \hbar\omega_\lambda$ is the signature of a strong vibrational instability. This situation corresponds to the population inversion condition described in the literature for donor−acceptor states.[7,35] Here, the applied voltage has driven the occupied left resonance above the empty right state. When the offset matches the energy of a vibrational mode, emission is greatly enhanced, and the junction can become unstable. However, the negative values to the right of Figure 5 show that vibrational instabilities are also possible outside this regime of population inversion. Results from DFT-NEGF for mode 2 (green circle) are matched by the model system and confirm the unstable character of the mode. This trend is observed for all unstable modes. These results show that, in molecular wires with separated unoccupied electronic states, vibrational instabilities can arise without the conditions of donor and acceptor states and population inversion.

To summarize, we demonstrated that current-induced vibrational instabilities are a much more general phenomenon than previously reported. We showed that they can be expected in molecular junctions with separated empty electronic states. We exemplified this regime in a junction where steric repulsion induces the twisting of benzene rings, resulting in decreased conjugation and states localized on either side of the molecule. In linear chains of conjugated rings lacking steric groups, this electronic separation also occurs when thermal fluctuations induce large twist angles during ring rotation. We calculated, combining DFT-NEGF and model calculations, the rates of absorption and emission of vibrations and analyzed several unstable modes. We characterized the unstable vibrational modes and presented a stability diagram for the electron-vibration coupling matrix elements. We also considered the effect of electronic structure, where we extended the previous findings beyond the condition of donor and acceptor states under population inversion. This study reveals the important role and interplay of electronic structure and electron-vibration coupling in the heating and cooling dynamics of a broad class of conjugated molecular wires.

■ ASSOCIATED CONTENT

Supporting Information

The Supporting Information is available free of charge on the ACS Publications website at DOI: 10.1021/acs.jpclett.8b00940.

Computational details, a real space representation of unstable modes, fitting of the transmission function, emission and absorption functions from model calculations, fitting of the electron-vibration coupling matrix, contributions to emission and absorption functions, fitting of stable modes, stability diagram for different values of electron-vibration coupling matrix and mode energies, stability diagram as a function of energy level offset, and self-consistent Born approximation (PDF)

■ AUTHOR INFORMATION

Corresponding Authors

*E-mail: foti@fzu.cz.

*E-mail: vazquez@fzu.cz.

ORCID

Giuseppe Foti: 0000-0001-5769-2253

Héctor Vázquez: 0000-0002-3865-9922

Notes

The authors declare no competing financial interest.

DOI: 10.1021/acs.jpclett.8b00940
J. Phys. Chem. Lett. 2018, 9, 2791−2796

■ ACKNOWLEDGMENTS

We gratefully acknowledge financial support from the Czech Science Foundation (GAČR) under Project 15-19672S, the Purkyně Fellowship program of the Academy of Sciences of the Czech Republic, and the European Union's Horizon 2020 research and innovation programme under the Marie Skłodowska-Curie Grant Agreement No. 709114. We thank the National Grid Infrastructure MetaCentrum for access to computing and storage facilities provided by the "Projects of Large Research, Development, and Innovations Infrastructures" (CESNET LM2015042) program.

■ REFERENCES

(1) Cuevas, J. C.; Scheer, E. *Molecular Electronics: An Introduction to Theory and Experiment*; World Scientific Publishing Co. Pte. Ltd.: Singapore, 2010.
(2) Su, T. A.; Neupane, M.; Steigerwald, M. L.; Venkataraman, L.; Nuckolls, C. Chemical principles of single-molecule electronics. *Nat. Rev. Mater.* **2016**, *1*, 16002.
(3) Galperin, M.; Ratner, M. A.; Nitzan, A. Molecular Transport Junctions: Vibrational Effects. *J. Phys.: Condens. Matter* **2007**, *19*, 103201.
(4) Huang, Z.; Chen, F.; D'agosta, R.; Bennett, P. A.; Di Ventra, M.; Tao, N. J. Local Ionic and Electron Heating in Single-Molecule Junctions. *Nat. Nanotechnol.* **2007**, *2*, 698−703.
(5) Ward, D. R.; Corley, D. A.; Tour, J. M.; Natelson, D. Vibrational and Electronic Heating in Nanoscale Junctions. *Nat. Nanotechnol.* **2011**, *6*, 33−38.
(6) Romano, G.; Gagliardi, A.; Pecchia, A.; Di Carlo, A. Heating and Cooling Mechanisms in Single-Molecule Junctions. *Phys. Rev. B: Condens. Matter Mater. Phys.* **2010**, *81*, 115438.
(7) Lü, J.-T.; Hedegård, P.; Brandbyge, M. Laserlike Vibrational Instability in Rectifying Molecular Conductors. *Phys. Rev. Lett.* **2011**, *107*, 046801.
(8) Franke, K. J.; Pascual, J. I. Effects of Electron-Vibration Coupling in Transport through Single Molecules. *J. Phys.: Condens. Matter* **2012**, *24*, 394002.
(9) Lee, W.; Kim, K.; Jeong, W.; Zotti, L. A.; Pauly, F.; Cuevas, J. C.; Reddy, P. Heat Dissipation in Atomic-Scale Junctions. *Nature* **2013**, *498*, 209−212.
(10) Kaasbjerg, K.; Novotný, T.; Nitzan, A. Charge-carrier-induced frequency renormalization, damping, and heating of vibrational modes in nanoscale junctions. *Phys. Rev. B: Condens. Matter Mater. Phys.* **2013**, *88*, 201405.
(11) Stipe, B. C.; Rezaei, M. A.; Ho, W. Inducing and Viewing the Rotational Motion of a Single Molecule. *Science* **1998**, *279*, 1907−1909.
(12) Liljeroth, P.; Repp, J.; Meyer, G. Current-Induced Hydrogen Tautomerization and Conductance Switching of Naphthalocyanine Molecules. *Science* **2007**, *317*, 1203−1206.
(13) Girit, Ç. Ö.; Meyer, J. C.; Erni, R.; Rossell, M. D.; Kisielowski, C.; Yang, L.; Park, C.-H.; Crommie, M. F.; Cohen, M. L.; Louie, S. G.; et al. Graphene at the Edge: Stability and Dynamics. *Science* **2009**, *323*, 1705−1708.
(14) Kumagai, T.; Hanke, F.; Gawinkowski, S.; Sharp, J.; Kotsis, K.; Waluk, J.; Persson, M.; Grill, L. Thermally and Vibrationally Induced Tautomerization of Single Porphycene Molecules on a Cu(110) Surface. *Phys. Rev. Lett.* **2013**, *111*, 246101.
(15) Kim, H.; Chang, Y. H.; Jang, W.-J.; Lee, E.-S.; Kim, Y.-H.; Kahng, S.-J. Probing Single-Molecule Dissociations from a Bimolecular Complex NO-Co-Porphyrin. *ACS Nano* **2015**, *9*, 7722−7728.
(16) Kim, Y.; Komeda, T.; Kawai, M. Single-Molecule Reaction and Characterization by Vibrational Excitation. *Phys. Rev. Lett.* **2002**, *89*, 126104.
(17) Schulze, G.; Franke, K. J.; Gagliardi, A.; Romano, G.; Lin, C. S.; Rosa, A. L.; Niehaus, T. A.; Frauenheim, T.; Di Carlo, A.; Pecchia, A.; Pascual, J. I. Resonant Electron Heating and Molecular Phonon Cooling in Single C_{60} Junctions. *Phys. Rev. Lett.* **2008**, *100*, 136801.
(18) Li, H.; Kim, N. T.; Su, T. A.; Steigerwald, M. L.; Nuckolls, C.; Darancet, P.; Leighton, J. L.; Venkataraman, L. Mechanism for Si-Si Bond Rupture in Single Molecule Junctions. *J. Am. Chem. Soc.* **2016**, *138*, 16159−16164.
(19) Segal, D.; Nitzan, A. Heating in current carrying molecular junctions. *J. Chem. Phys.* **2002**, *117*, 3915−3927.
(20) Koch, J.; Semmelhack, M.; von Oppen, F.; Nitzan, A. Current-induced nonequilibrium vibrations in single-molecule devices. *Phys. Rev. B: Condens. Matter Mater. Phys.* **2006**, *73*, 155306.
(21) Jorn, R.; Seideman, T. Competition between current-induced excitation and bath-induced decoherence in molecular junctions. *J. Chem. Phys.* **2009**, *131*, 244114.
(22) Härtle, R.; Thoss, M. Resonant electron transport in single-molecule junctions: Vibrational excitation, rectification, negative differential resistance, and local cooling. *Phys. Rev. B: Condens. Matter Mater. Phys.* **2011**, *83*, 115414.
(23) Tikhodeev, S. G.; Ueba, H. Relation between inelastic electron tunneling and vibrational excitation of single adsorbates on metal surfaces. *Phys. Rev. B: Condens. Matter Mater. Phys.* **2004**, *70*, 125414.
(24) Galperin, M.; Saito, K.; Balatsky, A. V.; Nitzan, A. Cooling Mechanisms in Molecular Conduction Junctions. *Phys. Rev. B: Condens. Matter Mater. Phys.* **2009**, *80*, 115427.
(25) Volkovich, R.; Hartle, R.; Thoss, M.; Peskin, U. Bias-controlled selective excitation of vibrational modes in molecular junctions: a route towards mode-selective chemistry. *Phys. Chem. Chem. Phys.* **2011**, *13*, 14333−14349.
(26) Dzhioev, A. A.; Kosov, D. S.; von Oppen, F. Out-of-equilibrium catalysis of chemical reactions by electronic tunnel currents. *J. Chem. Phys.* **2013**, *138*, 134103.
(27) Frederiksen, T.; Brandbyge, M.; Lorente, N.; Jauho, A.-P. Inelastic Scattering and Local Heating in Atomic Gold Wires. *Phys. Rev. Lett.* **2004**, *93*, 256601.
(28) Pecchia, A.; Romano, G.; Di Carlo, A. Theory of Heat Dissipation in Molecular Electronics. *Phys. Rev. B: Condens. Matter Mater. Phys.* **2007**, *75*, 035401.
(29) Lü, J.-T.; Gunst, T.; Hedegård, P.; Brandbyge, M. Current-induced dynamics in carbon atomic contacts. *Beilstein J. Nanotechnol.* **2011**, *2*, 814−823.
(30) Foti, G.; Vázquez, H. Interface Tuning of Current-Induced Cooling in Molecular Circuits. *J. Phys. Chem. C* **2017**, *121*, 1082−1088.
(31) Foti, G.; Vázquez, H. Adsorbate-driven cooling of carbene-based molecular junctions. *Beilstein J. Nanotechnol.* **2017**, *8*, 2060−2068.
(32) Härtle, R.; Thoss, M. Vibrational instabilities in resonant electron transport through single-molecule junctions. *Phys. Rev. B: Condens. Matter Mater. Phys.* **2011**, *83*, 125419.
(33) Dundas, D.; McEniry, E. J.; Todorov, T. N. Current-Driven Atomic Waterwheels. *Nat. Nanotechnol.* **2009**, *4*, 99−102.
(34) Sabater, C.; Untiedt, C.; van Ruitenbeek, J. M. Evidence for Non-Conservative Current-Induced Forces in the Breaking of Au and Pt Atomic Chains. *Beilstein J. Nanotechnol.* **2015**, *6*, 2338−2344.
(35) Simine, L.; Segal, D. Vibrational cooling, heating, and instability in molecular conducting junctions: full counting statistics analysis. *Phys. Chem. Chem. Phys.* **2012**, *14*, 13820−13834.
(36) Elbing, M.; Ochs, R.; Koentopp, M.; Fischer, M.; von Hänisch, C.; Weigend, F.; Evers, F.; Weber, H. B.; Mayor, M. A single-molecule diode. *Proc. Natl. Acad. Sci. U. S. A.* **2005**, *102*, 8815−8820.
(37) Zheng, W.; Wang, B.-B.; Li, C.-H.; Zhang, J.-X.; Wan, C.-Z.; Huang, J.-H.; Liu, J.; Shen, Z.; You, X.-Z. Asymmetric Donor-π-Acceptor-Type Benzo-Fused Aza-BODIPYs: Facile Synthesis and Colorimetric Properties. *Angew. Chem., Int. Ed.* **2015**, *54*, 9070−9074.
(38) Meier, T.; Pawlak, R.; Kawai, S.; Geng, Y.; Liu, X.; Decurtins, S.; Hapala, P.; Baratoff, A.; Liu, S.-X.; Jelínek, P.; et al. Donor-Acceptor Properties of a Single-Molecule Altered by On-Surface Complex Formation. *ACS Nano* **2017**, *11*, 8413−8420.

DOI: 10.1021/acs.jpclett.8b00940
J. Phys. Chem. Lett. 2018, 9, 2791−2796

(39) Venkataraman, L.; Klare, J. E.; Nuckolls, C.; Hybertsen, M. S.; Steigerwald, M. L. Dependence of single-molecule junction conductance on molecular conformation. *Nature* **2006**, *442*, 904−907.
(40) Mishchenko, A.; Zotti, L. A.; Vonlanthen, D.; Bürkle, M.; Pauly, F.; Cuevas, J. C.; Mayor, M.; Wandlowski, T. Single-Molecule Junctions Based on Nitrile-Terminated Biphenyls: A Promising New Anchoring Group. *J. Am. Chem. Soc.* **2011**, *133*, 184−187.
(41) Gunst, T.; Lü, J.-T.; Hedegård, P.; Brandbyge, M. Phonon Excitation and Instabilities in Biased Graphene Nanoconstrictions. *Phys. Rev. B: Condens. Matter Mater. Phys.* **2013**, *88*, 161401.
(42) Foti, G.; Vázquez, H. Interface Tuning of Current-Induced Cooling in Molecular Circuits. *J. Phys. Chem. C* **2017**, *121*, 1082−1088.
(43) Quek, S. Y.; Khoo, K. H. Predictive DFT-Based Approaches to Charge and Spin Transport in Single-Molecule Junctions and Two-Dimensional Materials: Successes and Challenges. *Acc. Chem. Res.* **2014**, *47*, 3250−3257.

DOI: 10.1021/acs.jpclett.8b00940
J. Phys. Chem. Lett. 2018, 9, 2791−2796